University of Kentucky
UKnowledge

Pharmaceutical Sciences Faculty Publications | Pharmaceutical Sciences

1-2014

Programmable folding of fusion RNA *in vivo* and *in vitro* driven by pRNA 3WJ motif of phi29 DNA packaging motor

Dan Shu
University of Kentucky, dan.shu@uky.edu

Emil F. Khisamutdinov
University of Kentucky, emil.k@uky.edu

Le Zhang
University of Kentucky, le.zhang@uky.edu

Peixuan Guo
University of Kentucky, peixuan.guo@uky.edu

Right click to open a feedback form in a new tab to let us know how this document benefits you.

Follow this and additional works at: https://uknowledge.uky.edu/ps_facpub

Part of the Pharmacy and Pharmaceutical Sciences Commons

Programmable folding of fusion RNA *in vivo* and *in vitro* driven by pRNA 3WJ motif of phi29 DNA packaging motor

Digital Object Identifier (DOI)
http://dx.doi.org/10.1093/nar/gkt885

Notes/Citation Information

Published in *Nucleic Acids Research*, v. 42, issue 2, no. e10.

© The Author(s) 2013. Published by Oxford University Press.

This is an Open Access article distributed under the terms of the Creative Commons Attribution Non-Commercial License (http://creativecommons.org/licenses/by-nc/3.0/), which permits non-commercial re-use, distribution, and reproduction in any medium, provided the original work is properly cited. For commercial re-use, please contact journals.permissions@oup.com.

This article is available at UKnowledge: https://uknowledge.uky.edu/ps_facpub/17

Published online 30 September 2013 Nucleic Acids Research, 2014, Vol. 42, No. 2 e10
doi:10.1093/nar/gkt885

Programmable folding of fusion RNA *in vivo* and *in vitro* driven by pRNA 3WJ motif of phi29 DNA packaging motor

Dan Shu, Emil F. Khisamutdinov, Le Zhang and Peixuan Guo*

Nanobiotechnology Center, Markey Cancer Center, and Department of Pharmaceutical Sciences, College of Pharmacy, University of Kentucky, Lexington, KY 40536, USA

Received July 30, 2013; Revised September 6, 2013; Accepted September 9, 2013

ABSTRACT

Misfolding and associated loss of function are common problems in constructing fusion RNA complexes due to changes in energy landscape and the nearest-neighbor principle. Here we report the incorporation and application of the pRNA-3WJ motif of the phi29 DNA packaging motor into fusion RNA with controllable and predictable folding. The motif included three discontinuous ~18 nucleotide (nt) fragments, displayed a distinct low folding energy (Shu D *et al.*, *Nature Nanotechnology*, 2011, 6:658–667), and folded spontaneously into a leading core that enabled the correct folding of other functionalities fused to the RNA complex. Three individual fragments dispersed at any location within the sequence allowed the other RNA functional modules to fold into their original structures with authentic functions, as tested by Hepatitis B virus ribozyme, siRNA, and aptamers for malachite green (MG), spinach, and streptavidin (STV). Only nine complementary nucleotides were present for any two of the three ~18-nt fragments, but the three 9 bp branches were so powerful that they disrupted other double strands with more than 15 bp within the fusion RNA. This system enabled the production of fusion complexes harboring multiple RNA functionalities with correct folding for potential applications in biotechnology, nanomedicine and nanotechnology. We also applied this system to investigate the principles governing the folding of RNA *in vivo* and *in vitro*. Temporal production of RNA sequences during *in vivo* transcription caused RNA to fold into different conformations that could not be predicted with routine principles derived from *in vitro* studies.

INTRODUCTION

RNA nanotechnology involves programmable and addressable designs of RNA 3D nanoparticles by fusing or grafting individual RNA structural moieties or functionalities to one another (1,2). Many RNA folding programs are available (3–5) for RNA secondary structure prediction. However, manipulating tertiary folding of the reconstructed RNA is very challenging due to changes in the nearest-neighbor and the redistribution of energy landscapes. Development of systems to fold RNA functionalities in a controllable and predictable manner is therefore very desirable. It has been reported that RNA junction motifs, such as the three-way junction (3WJ) (6–9), four-way junction (4WJ) (10), and five-way junction (5WJ) (11) can form stable conformations composed of discontinuous RNA fragments. For example, the stable properties of the 3WJ structural motif derived from pRNA of bacteriophage phi29 DNA packaging motor has been utilized to generate functional RNA nanoparticles (6–8,12). Other examples of *in silico* generated RNA nanostructures based on RNA structural motifs include RNAI/II inverse kissing loops (13), kink-turn structural motifs (14,15), receptor-loop/loop-receptor interacting motifs (16,17), and phi29 pRNA hand-in-hand and foot-to-foot interactions (1,12, 18–22). In addition, tightly folded RNA motifs have been reported *in vivo* that served as vectors to carry exogenous functional RNA modules (23).

More and more non-coding RNA molecules have been discovered to play essential roles in the regulation of a variety of diverse biological functions in cells (24–27). Often, the function of an RNA molecule is dependent on its tertiary structure, as well as information encoded in its canonical or non-canonical base pairing (28–30). Thus, prior to *in vitro* or *in vivo* design of artificial RNA nanoparticles, one needs to consider if the desired fusion RNA will fold into the predicted functional structure and retain its correct functionality. An example is the RNA paranemic motif coupled with malachite green (MG)

*To whom correspondence should be addressed. Tel: +1 859 218 0128; Fax: +1 859 257 1307; Email: peixuan.guo@uky.edu

© The Author(s) 2013. Published by Oxford University Press.
This is an Open Access article distributed under the terms of the Creative Commons Attribution Non-Commercial License (http://creativecommons.org/licenses/by-nc/3.0/), which permits non-commercial re-use, distribution, and reproduction in any medium, provided the original work is properly cited. For commercial re-use, please contact journals.permissions@oup.com

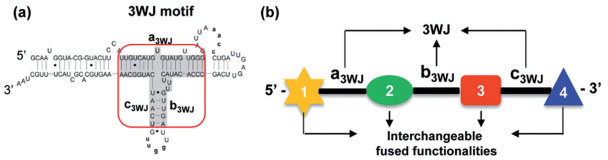

Figure 1. Experimental design for the construction of fusion RNA complexes harboring multiple functionalities driven by pRNA-3WJ core. (**a**) Secondary structure of the pRNA from the bacteriophage phi29 DNA packaging motor. The central 3WJ motif is boxed. (**b**) Approach for the construction of fusion RNA complexes. In the figure, a_{3WJ}, b_{3WJ}, and c_{3WJ} represent the three strands of the pRNA-3WJ complex; *1–4* represent RNA functional modules.

binding RNA aptamer (31) to confer rigidity and enhance fluorescence emission (6,7,8,32).

The structural properties encoded in intracellular functional RNAs are extremely important in RNA nanotechnology. Several methods have been applied to determine structural properties of small and large RNAs (33–37), including physical and chemical approaches to probe RNA/ribonucleoprotein structures *in vitro* (38). Additionally, several chemical reagents that are sensitive to secondary and/or tertiary structures have been used for elucidating RNA structure *in vivo* (34). Dimethyl sulfate (DMS) has been extensively applied for probing RNA structure in a variety of organisms ranging from bacteria to eukaryotes (39,40). Lead-(II)-acetate has also been used to probe RNA structures in bacteria (41); this ion easily enters bacterial cells and primarily induces specific cleavages at positions of tight metal ion binding. Another chemical reagent is the hydroxyl radical (OH), which has been widely used in nucleic acid footprinting (42). This technique can be applied to probe RNA tertiary structure and its intermolecular interactions.

Recently, we discovered that the pRNA-3WJ motif (Figure 1a) exhibits unusually robust properties (6,8,43) and can serve as a core to drive the folding of other RNA molecules fused to the complex. The pRNA-3WJ domain can be assembled from three pieces of RNA oligonucleotides resulting in a structure with: (i) an unusually high thermodynamic stability; (ii) highly efficient complex assembly even in the absence of metal salts; (iii) resistance to denaturation even in the presence of 8 M urea; (iv) the ability to stay intact without dissociating at ultra-low concentrations; and (v) coordination of two divalent metal ions (6,43). Herein, we demonstrate that this robust pRNA-3WJ motif can provide a leading core and drive the correct folding of other functionalities fused into the RNA complex with controllable and predictable consequences. This system will enable the production of fusion RNA with incorporated functionalities folded into their authentic structure and function for applications in biotechnology and nanotechnology.

MATERIALS AND METHODS

In vitro synthesis and purification of RNAs

All pRNA-3WJ constructs were prepared by *in vitro* transcription using T7 RNA polymerase from DNA templates amplified by polymerase chain reaction (PCR), as described previously (44). The DNA templates and primers were synthesized chemically by IDT (Iowa). RNAs were used directly for MG fluorescence assays, or purified by 8 M urea 8% polyacrylamide gel electrophoresis (PAGE).

Folate binding assay

Human nasopharyngeal carcinoma KB cells [American Type Culture Collection (ATCC)] were grown on glass coverslides in folate-free medium overnight. Cy3-labeled pRNA-3WJ-FA-siRNA(survivin)-Ribozyme was incubated with the cells at 37°C for 2 h. After washing with phosphate buffered saline (PBS), the cells were fixed by 4% paraformaldehyde and stained by Alexa Fluor® 488 phalloidin (Invitrogen) for cytoskeleton and TO-PRO®-3 iodide (642/661) (Invitrogen) for nucleus. The cells were then assayed for binding and cell entry by Zeiss LSM 510 laser scanning confocal microscope.

Assay for the silencing of genes in cancer cell model

KB cells were transfected with 25 nM of individual fusion pRNA-3WJ complex using Lipofectamine 2000 Transfection Reagent (Invitrogen). After 48 h, cells were collected and target gene silencing effects were assessed by western blot assay, as previously described (6). Briefly, cells were lysed by Radio-Immunoprecipitation Assay (RIPA) lysis buffer (Sigma) and the cell total protein was extracted for the assay. Equal amounts of proteins were then loaded onto 15% sodium dodecyl sulfate (SDS)–PAGE and electrophoretically transferred to Immun-Blot PVDF membranes (Bio-rad). The membrane was probed with *survivin* antibody (R&D) (1:4000 diluted) and β-actin antibody (Sigma) (1:5000 diluted) overnight, followed by 1:10 000 anti-rabbit secondary antibody conjugated with horseradish peroxidase (Millipore) for 1 h. Membranes were blotted by ECL kits (Millipore) and exposed to film for autoradiography.

Binding assay for the Streptavidin-binding aptamer

Tritium-labeled [^{3}H] RNA nanostructures (pRNA-3WJ-MG-HBV-STV) were preassembled in binding buffer (PBS with 10 mM Mg^{2+}) before incubation with streptavidin (STV) agarose resin (Thermo Scientific). A total of 50 µl aliquot of STV resin was equilibrated at room temperature (RT) following washing with binding buffer. In all, ~5 µg RNA samples were added to each tube and incubated with the resin for 1 h at RT. After incubation, the resin was spun at 500 × g for 1 min, and the supernatant (pass through) was removed. Then, 50 µl binding buffer was added to the mixture and incubated for 15 min to wash the resin several times. RNA was eluted by 5 mM biotin solution and samples were analyzed on a 1900 TR Liquid Scintillation Counter (Packard).

Hepatitis B virus ribozyme activity assay

Hepatitis B virus (HBV) substrate was labeled with Cy3 (Mirus Bio LLC) and incubated with RNA nanoparticle at 37°C for 1 hr in Tris buffer (50 mM Tris–HCl, pH = 7.5; 20 mM $MgCl_2$, 20 mM NaCl). pRNA-HBV ribozyme was used as a positive control (45). After

incubation, the products were run in 8 M Urea, 10% PAGE gel for fluorescence imaging.

MG aptamer fluorescence assay

Gel-purified RNAs were mixed with 2 μM Malachite Green, tremethylmetane (MG) in binding buffer containing 100 mM KCl, 5 mM $MgCl_2$ and 10 mM HEPES (pH 7.4) and incubated at RT for 30 min. The refolded RNA samples were heating to 95°C for 5 min followed by slow cooling to 37°C prior to MG staining. Fluorescence was measured using a fluorospectrometer (Horiba Jobin Yvon; SPEX Fluolog-3), excited at 615 nm, scanning from 625 to 800 nm for emission (7,32,46).

Spinach fluorescence measurements

Assembled pRNA-3WJ nanoparticles (0.2 μM) fused with Spinach aptamer in TMS buffer were mixed with DFHBI dye (2 μM) and incubated at room temperature for 30 min. Fluorescence was measured using a fluorospectrometer (Horiba Jobin Yvon), excited at 450 nm and scanning from 565 to 750 nm for emission.

Vector construction for *in vivo* expression

A sequence of cis-ribozyme was fused onto the 3′-end of DNA templates of corresponding RNA for terminal processing (45,46). The *5′ + 0* (Reference), *5′ + 6*, *5′ + 12*, and *5′ + 15* were inserted between BglII/NdeI sites of expression vector pET-3b. BglII cleavage removed the original T7 promoter in the vector to prevent any undesired sequence in the 5′-end of the RNA product. The insertion fragment contained the T7 promoter at the 5′-end. The clone was transformed into *Escherichia coli* strain DH5α and recombinant plasmids were verified by sequencing (GENEWIZ).

RNA *in vivo* expression and purification

Escherichia coli strain BL21 star (DE3; Invitrogen) was transformed by the recombinant plasmids, and the colony was inoculated by 5 ml LB medium containing 100 μg/ml ampicillin, grown at 37°C, and shaken at 250 rpm until $A_{600\ nm}$ reached 0.5. IPTG solution of 50 μl (1 M) was added to 5 ml of cell culture. Cells were allowed to grow for 1.5 h, and then were pelleted and resuspended in 250 μl of 10 mM magnesium acetate, 1 mM Tris–HCl, pH 7.4 (47). The total soluble RNAs were extracted using 500 μl of water saturated phenol (pH 4.5; Fisher). The aqueous phase was ethanol precipitated then dissolved in 50 μl of 0.05% DEPC treated water.

Gel electrophoresis of *in vivo* prepared RNAs

In vivo expressed *5′ + 0* (reference), *5′ + 6*, *5′ + 12*, and *5′ + 15* RNAs were analyzed by 8% PAGE gel containing 8 M of urea by loading 5 μl of each sample and run in 1x TBE (89 mM Tris base, 89 mM Boric acid, 2 mM ethylenediaminetetraacetic acid) at 120 V, at RT for 1 h. The 8% native PAGE gel was run in 1x TBM (89 mM Tris base, 200 mM Boric acid, 5 mM $MgCl_2$, pH 8.0) at 70 V, at 4°C for 3 h. After electrophoresis, the gels were stained with 10 μM MG in 100 mM KCl, 5 mM $MgCl_2$, and 10 mM HEPES (pH 7.4) for 15 min at RT. The MG fluorescence image was acquired by the Cy5 channel (635 nm excitation/670 nm emission) using a Typhoon scanner (48). The gels were then stained with EB and scanned in EB channel (532 nm excitation/580 nm emission).

RESULTS

pRNA-3WJ motif drives the folding of different RNA functionalities in fusion RNA

Figure 1b shows the design principles for constructing fusion RNA with multiple functionalities. The three pRNA-3WJ fragments (a_{3WJ}, b_{3WJ}, and c_{3WJ}) are dispersed within the complex and serve as a driving force for the folding of other RNA molecules. Several RNA functionalities were incorporated and tested *in vitro* including: (i) siRNA targeting survivin gene (49,50); (ii) MG (Malachite Green dye, triphenylmethane) binding RNA aptamer (51); (iii) Spinach RNA aptamer (52); (iv) STV binding RNA aptamer (53); and (v) HBV ribozyme (45). These RNA moieties are unique in their sequences and folding properties, and exhibit different Gibbs free energies (ΔG). When the functional therapeutic RNA moieties, i.e. siRNA, ribozymes or receptor-binding aptamers, were fused to any of the three branches of the pRNA-3WJ, the 3WJ and the incorporated RNA modules folded independently, as validated by AFM image (Figure 2a), and retained their authentic functions, as demonstrated by functional assays (Figure 2). The location of the three 3WJ fragments in the fusion RNA was not critical; but the order of appearance from 5′- a_{3WJ}, to b_{3WJ}, to c_{3WJ} -3′ (Figure 1b) was the essential factor.

Assessment of cell binding and gene silencing using fusion pRNA-3WJ-FA-siRNA (survivin)-Ribozyme nanoparticles

A pRNA-3WJ complex was coupled with folate (FA) ligand, survivin siRNA, and ribozyme, denoted as pRNA-3WJ-Folate-siRNA(survivin)-Ribozyme nanoparticle (Figure 2a). FA serves as a cancer cell delivery agent *via* receptor mediated endocytosis (6,8,54). Cy3-labeled pRNA-3WJ complex was incubated with FA-receptor positive KB cells and tested for cell binding efficiency. Confocal microscopy indicated strong binding of RNA nanoparticles as demonstrated by excellent co-localization of cytoplasma (green) and RNA nanoparticles (red) (Figure 2b).

Western blot was performed to assay the gene silencing effects of survivin siRNA in KB cells. After 48-h transfection, reduced survivin protein expression level was observed compared to scramble controls (Figure 2c). β-actin was used as an endogenous control. We previously demonstrated that the mechanism of siRNA release from pRNA nanoparticles is by Dicer processing (21).

Assessment of aptamer functionalities using fusion pRNA-3WJ-MG-Spinach nanoparticles

MG binding RNA aptamers (51) and Spinach RNA aptamers (52) were fused to the pRNA-3WJ scaffold (denoted pRNA-3WJ-MG-Spinach nanoparticles) for structure and function verification (Figure 2d). Free

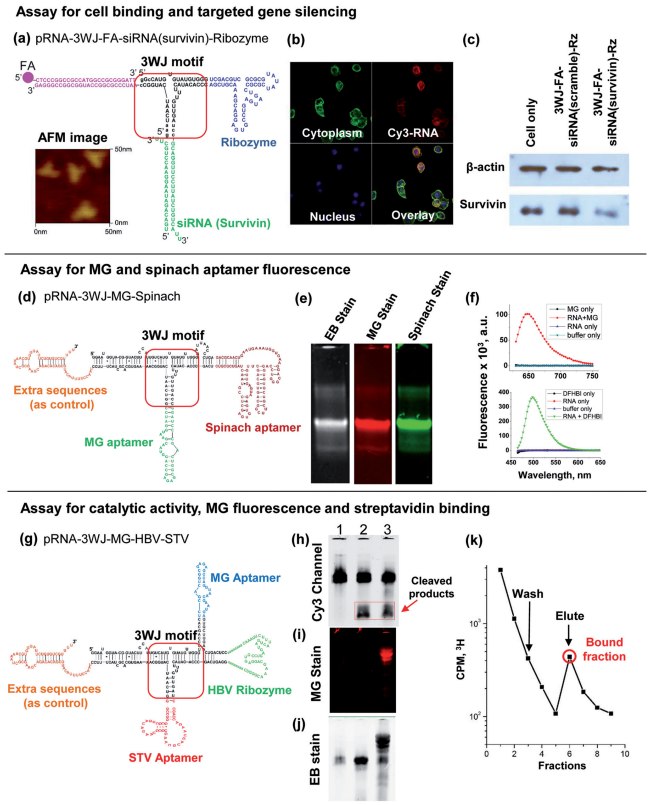

Figure 2. Functional assays of fusion RNA complexes harboring multiple functionalities. (**a**) Construction of RNA complex harboring folate (FA), survivin siRNA, and ribozyme (denoted, pRNA-3WJ-FA-siRNA (survivin)-Ribozyme) and corresponding AFM image. (**b**) Confocal images showing the targeting of FA-receptor positive KB cells by colocalization of cytoplasm (green) and RNA nanoparticles (red). Blue represents nuclei. (**c**) Western blot assay showing target knockdown of survivin protein by siRNA. β-actin serves as endogenous control. (**d**) Construction of RNA complex harboring malachite green (MG) (6–8,32,51) binding and Spinach aptamer (denoted, pRNA-3WJ-MG-Spinach) (52). (**e**) The 8% native PAGE verifying the fluorogenic properties of the two RNA aptamers. (**f**) Fluorescence spectra of MG aptamer (top) and Spinach aptamer (bottom) in solution, measured by fluorospectrometer. (**g**) Construction of RNA complex harboring MG aptamer, HBV ribozyme, and streptavidin aptamer (pRNA-3WJ-MG-HBV-STV). (**h**) The 8% native PAGE gel showing the catalytic activity of the incorporated HBV ribozyme. (**i**) MG aptamer activity verified by MG staining. (**j**) EB staining to verify the presence of RNA nanoparticles. (**k**) STV binding assay using STV affinity column (53). Bound RNA complexes were eluted by adding 5 mM biotin (outlined in red).

MG and DFHBI (3,5-difluoro-4-hydroxybenzylidene imidazolinone; Spinach aptamer-binding dye) are not fluorescent by themselves, and only emit fluorescence after binding to the correctly folded RNA aptamers. Both MG binding aptamer and Spinach aptamers incorporated in the 3WJ motif retained their capacity to bind MG and DFHBI dyes, respectively, as demonstrated by their fluorescence emission in native PAGE (Figure 2e) and in solution (Figure 2f).

Assessment of ribozyme catalytic activity and STV binding using fusion pRNA-3WJ-MG-HBV-STV nanoparticles

Tetravalent RNA nanoparticles were constructed using pRNA-3WJ motif harboring MG binding aptamer (6,8,32), HBV ribozyme (45), and STV aptamer (53,48) (denoted pRNA-3WJ-MG-HBV-STV nanoparticles) (Figure 2g). HBV ribozyme (45) was able to cleave its 135-nt RNA genome substrate into two fragments (60 nt and 75 nt) (Figure 2h). The results are comparable to optimized positive controls, thereby confirming that the fused ribozyme retained its authentic structure and function. MG aptamer also retained its capacity to bind MG dye, as revealed by fluorescence emissions in urea PAGE (Figure 2i) and verified by total RNA staining with EB (Figure 2j).

For assessment of STV binding, [^{3}H]-UTP whole chain labeled pRNA-3WJ-MG-HBV-STV nanoparticles were incubated with STV resin in an affinity column. The column was washed, and the RNA nanoparticles were then eluted with biotin (Figure 2k), indicating correct folding of the incorporated STV aptamer. As a negative control, RNA nanoparticles without STV aptamer did not appear in the elution fractions.

Design principles for evaluating the power of three pRNA-3WJ fragments to override other complementary sequences within fusion RNA constructs

The energy landscape and nearest-neighbor principle are key factors governing RNA folding. Due to the free-energy minimization principle, complementary sequences within RNA also play a critical role in the formation of RNA 3D structures, e.g. pseudoknots, multi-way junctions, and hairpins. To apply the pRNA-3WJ for fabricating RNA nanostructures, the power of three pRNA-3WJ fragments to override other complementary sequences within fusion RNA complexes have to be tested. Accordingly, fusion RNA complexes were designed based on: (i) three fragments of pRNA-3WJ to direct the folding of the RNA; (ii) additional 5′-end interfering sequences complementary to the internal sequence of the 3WJ; and (iii) MG-aptamer to serve as a reporter for verification of authentic folding (7). If the RNA is degraded or misfolded, the MG fluorescence will disappear, and therefore can be used as an indicator for assessing the folding of fusion RNA complexes.

RNA constructs containing interfering sequences have a designated nomenclature. For instance, '*5′ + 12* means that 12 overhanging nucleotides complementary to the MG-aptamer sequence were added at the 5′-end of the RNA complex. Similarly, '*5′NM + 12* (NM = non-matching) means that 12 nucleotides non-complementary to the MG-aptamer sequences were added at the 5′-end of the RNA complex. All RNA nanostructures were constructed to contain the pRNA-3WJ and an MG aptamer (Figure 3a). Because the sequence at the 5′-end appeared earlier during transcription than the sequence at the 3′-end, single-stranded (ss) nucleotides of different lengths (6, 12, and 15 nt) were added to the 5′-end, complementary to the MG-aptamer sequence, in order to interfere with the original folding driven by the pRNA-3WJ (Figure 3b). Several controls were designed in which overhanging NM nucleotides of differing lengths complementary to the MG-aptamer sequence were added (Figure 3c). All these

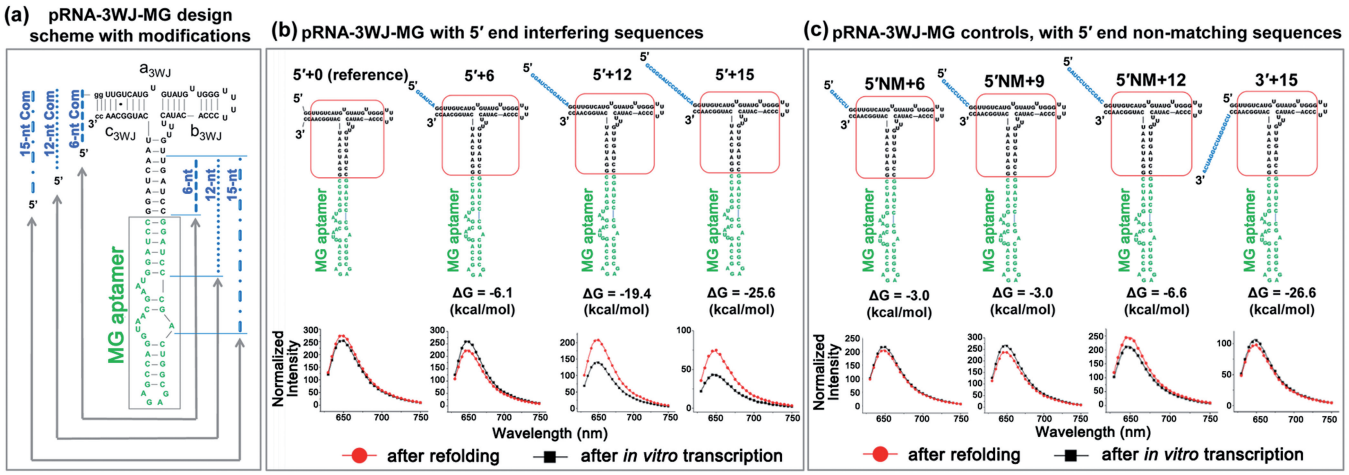

Figure 3. Design principles for evaluating the power of three pRNA-3WJ fragments to override other complementary sequences within fusion RNA constructs. (**a**) Schematic of the pRNA-3WJ structures showing location of the interfering nucleotides (left) and their complementary target (right). The 2D structures of the RNA complexes with 6, 12, or 15-nt interfering sequences (**b**) or scramble sequence (NM stands for non-matching) (**c**) at the 5′-end (top panel) and corresponding fluorescence spectra (bottom panel). In (b) and (c), black and red curves represent fluorescence spectra after transcription and after refolding, respectively.

RNA constructs contain discontinuous motifs, such as those observed in a pseudoknot (55–59).

We then investigated whether the folding was affected by the discontinuous motifs prior to or after refolding subsequent to transcription. This is particularly important in the context of *in vivo* folding of RNA and for transcribing therapeutic RNA nanoparticles directly in the cell with unprocessed additional sequences at the 5′- or 3′-ends. Measurements of fluorescence signals of RNA complexes directly after *in vitro* transcription for all pRNA-3WJ constructs suggested folding of authentic MG-aptamer reporter system embedded within the pRNA-3WJ (Figure 3b and c, black curves). These results revealed that even with only nine complementary nucleotides within the 3WJ, the folding power of the three 3WJ fragments could override more than 15 completely complementary nucleotides that could form double-stranded RNA within the RNA complex.

In addition, a control experiment was performed in which the MG fluorescence intensity of the *5′+12* constructs was compared to the construct where the 3WJ motif was destroyed by deletion of the a_{3WJ} strand (Figure 4). The lower intensity of the control RNA complex suggests that the folding of the MG aptamer was indeed affected by the disruption of the 3WJ, thereby confirming that all 3WJ component strands need to be present to drive the folding of other RNA modules into their fully functional state.

Comparison of pRNA-3WJ folding after transcription and after refolding

To unravel the folding differences of *in vitro* RNA transcription products before and after refolding, pRNA-3WJ-MG emission spectra were measured. RNA transcription reactions were performed, as described previously (60). The reactions were stopped by the addition of DNase I. Fluorescence spectra of the transcribed pRNA-3WJ-MG complex was then measured in the presence of MG fluorophore. The pRNA-3WJ-MG complex was then heated to 95°C and slowly cooled to 37°C (refolding). The fluorescence spectra of the refolded pRNA-3WJ-MG complex was then compared with the transcribed complex.

The fluorescence intensity was similar for all the control RNA samples, *5′+0*, *5′NM+6*, *5′NM+9*, and *5′NM+12*, regardless of the refolding step (Figure 3c). However, RNA constructs *5′+12* and *5′+15* with 12 and 15 overhanging nucleotides, respectively, showed significant differences (Figure 3b). Upon increasing the ssRNA length at the 5′-end from 6 to 12 nt, as exemplified in molecule *5′+12*, the fluorescence intensity after transcription was found to be lower than after refolding. Increasing the length of the ssRNA to 15-nt in RNA *5′+15* resulted in a larger difference (Figure 3b). These results demonstrate that the complementary interfering sequences at the 5′-end partially disrupted the folding of pRNA-3WJ assembly during the transcription reaction. In contrast, if the 15-nt complementary interfering sequence is instead placed at the 3′-end, no differences in fluorescence intensity are observed (Figure 3C, complex *3′+15*), which is consistent with our interpretations.

Ratio of fluorescence signals of pRNA-3WJ prior to and after refolding

To assess the folding differences of the pRNA-3WJ prior to and after refolding, the integrated areas of individual fluorescence signals of RNA constructs were measured before and after refolding. The fluorescence ratio ‘r’ was obtained for each RNA sample by dividing the integrated area at 37°C (after transcription) by the integrated area after heating to 95°C (after refolding). These ratios were calculated from a minimum of four individual experiments (Table 1). The ‘r’ value reflects the impact of discontinuous motifs on the folding properties of pRNA-3WJ as a function of the length of the interfering sequence during transcription and after refolding (Figure 5). RNA constructs with non-matching sequences to the MG-aptamer region, or with interfering sequences at the 3′-end, had

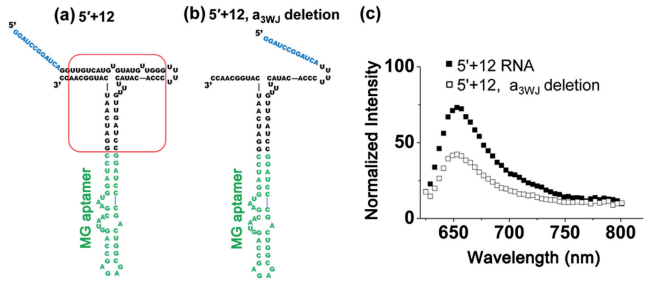

Figure 4. MG fluorescence intensity of the *5′ + 12* RNA construct compared to the construct where the 3WJ motif was destroyed by deletion of the a_{3WJ} strand. (**a–b**) The 2D structures of the *5′ + 12* RNA complexes without (a) and with (b) deletion of a_{3WJ} strand. (**c**) Comparison of MG fluorescence spectra for RNA constructs in (a) and (b).

Table 1. Ratio ('r') values of RNA nanostructures after transcription and after refolding

RNA	ssRNA length (nt)		Ratio (37°C/95°C)
	5′-end	3′-end	
5′ + 15	15	–	0.49 ± 0.07
5′ + 12	12	–	0.83 ± 0.08
5′ + 6	6	–	1.26 ± 0.20
5′ + 0	–	–	1.06 ± 0.20
5′NM + 12	12	–	1.28 ± 0.30
5′NM + 9	9	–	1.39 ± 0.30
5′NM + 6	6	–	1.29 ± 0.20
3′NM + 15	–	15	1.31 ± 0.30

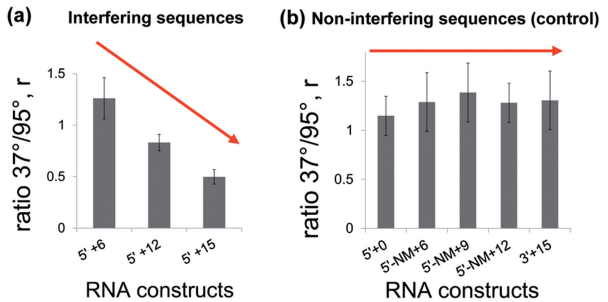

Figure 5. Correlation between the length of the interfering sequence and the ratio of fluorescence signals after transcription and after refolding. (**a**) Descending trend of the ratio of fluorescence signals before and after refolding in accordance with the increasing length of the 5′-end interference sequences. (**b**) Control complexes with scrambled or non-matching sequences do not exhibit any change.

similar 'r' values close to 1, indicating the effect was not dependent on nucleotide length (Figure 5b). However, in the presence of overhanging nucleotides that interfered with the MG-aptamer sequence there was a correlation: the longer the additional sequences at the 5′-end, the smaller the 'r' value, implying that there are fewer pRNA-3WJ-MG constructs that folded properly during temporal transcription (Figure 5a). The data leads to the conclusion that the RNA folding was temporally dependent. The 5′-end sequences that appeared earlier during transcription influenced the RNA folding more than the sequences that appeared later during transcription.

In vivo assessment of the effect of temporal folding after transcription

RNA constructs with interfering sequences of 6, 12, and 15 nt, similar to the *in vitro* design of the *5′ + 0*, *5′ + 6*, *5′ + 12*, and *5′ + 15* RNA were expressed in *E. coli* cells. The principle of this design was based on the following ideas: (i) a thermodynamically stable and tightly folded pRNA-3WJ would drive the correct folding of the MG-aptamer; (ii) tightly folded RNA are relatively resistant to RNase degradation in the cell (most cellular RNases degrade ssRNA, but not dsRNA) and misfolded RNA would be trimmed or truncated by RNase, leading to a loss in fluorescence from the MG dye that only binds to the appropriately folded and intact MG aptamer; and (iii) the assay would be based on the comparison of the sequences that affect the folding of the core of the pRNA-3WJ-MG-aptamer. Thus, a *cis*-acting ribozyme sequence was placed at the 3′-end to cleave the undesired sequences arising from uncontrolled termination of transcription at the 3′-end (Figure 6a) (45,61).

The RNA products from *E. coli* cells were first assayed by 8% denaturing PAGE (Figure 6b). As reported previously, the pRNA-3WJ is resistant to 8 M urea denaturation (6,8), and as such, denaturing gel can be used to detect the presence of the pRNA-3WJ-MG-aptamer complex. Upon staining with either ethidium bromide (EB) (Figure 6b, top) or MG dye (Figure 6b, bottom), the *5′ + 0* RNA, serving as a reference molecule, and the *5′ + 6* RNA were detected on the gel as distinct bands around 200 bp, indicating the presence of both the pRNA-3WJ and the MG-aptamer in both constructs. The higher yield of *5′ + 0* RNA compared to *5′ + 6* construct indicated that the 6 complementary nucleotides at the 5′-end of *5′ + 6* were able to disrupt the folding of the pRNA-3WJ-MG-aptamer complex only to some extent. However, MG-stained RNA was not detected in both *5′ + 12* and *5′ + 15* RNA lanes, indicating the misfolding of those pRNA-3WJ-MG-aptamer complexes. Several degraded products were observed between 50 and 70 bp after EB staining (Figure 6b, top, lanes *5′ + 12* and *5′ + 15*). This data agreed with the *in vitro* data, suggesting that RNA folding is temporally dependent during transcription, and that the 5′-end sequence appearing earlier during transcription influenced the RNA folding more than the sequence that appeared later during transcription.

To verify the denaturing PAGE results, fluorescence intensities of the RNA constructs obtained *in vivo* were measured further in presence of MG dye (Figure 6c), in a manner similar to that of the *in vitro* experiments (Figure 3). The fluorescence intensities were detected for both *5′ + 0* and *5′ + 6* constructs (Figure 6c, black curves). But, the *5′ + 0* RNA showed higher fluorescence value than the *5′ + 6* construct with six interfering nucleotides. There was almost no fluorescence detected for constructs *5′ + 12* and *5′ + 15*. These data are consistent with MG-stained denaturing PAGE, suggesting that while six interfering nucleotides partially disrupted the folding of pRNA-3WJ-MG-aptamer, 12 and 15 nt complementary

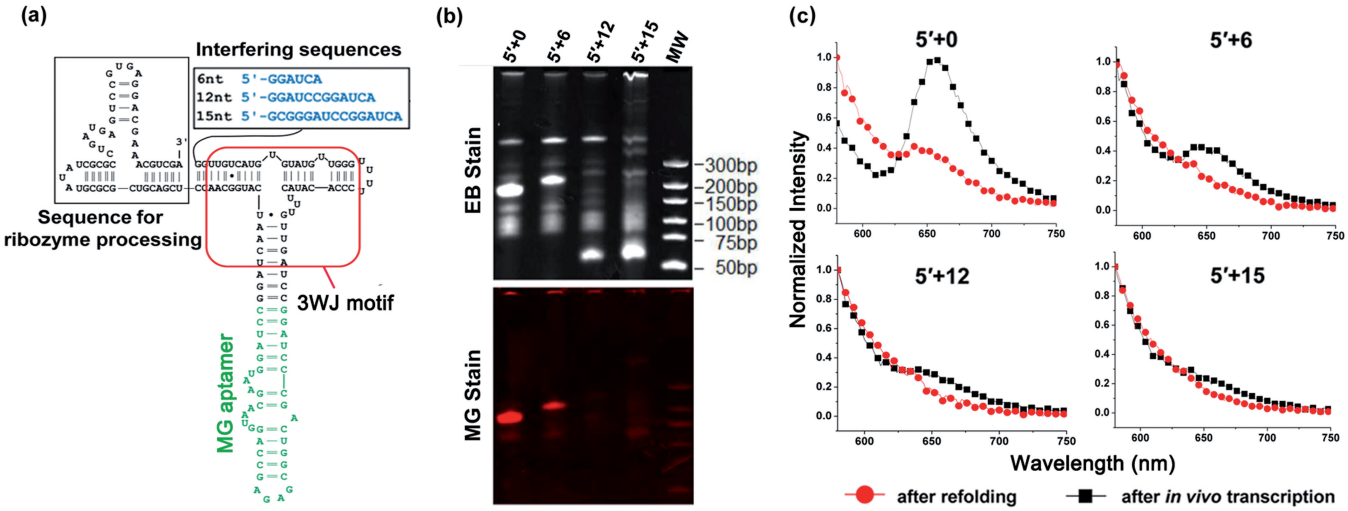

Figure 6. *In vivo* study of 3WJ-MG RNA complexes with 5′-end interfering sequences. (**a**) Design of *in vivo* study of RNA complexes with *cis*-acting ribozyme, MG aptamer, and interfering sequences. (**b**) MG folding assayed by 8% denaturing PAGE gel stained by EB and MG. Total soluble RNA fraction were extracted from *E. coli* after 1.5 h of IPTG induction. (**c**) Normalized fluorescence intensities of the *in vivo* expressed RNA constructed after transcription (black) and after refolding (red) for *5′+0*, *5′+6*, *5′+12,* and *5′+15* RNA constructs.

sequences completely interfered with the formation of pRNA-3WJ-MG-aptamer structures *in vivo*.

To refold the *in vivo* RNA products of pRNA-3WJ-MG-aptamer, the denaturation and refolding step was performed by heating the RNA solution to 95°C and slowly cooling to 37°C. Interestingly, the measured fluorescence intensities were significantly reduced or were not detected at all (Figure 6c, red curves). These data are in sharp contrast to that obtained from the *in vitro* experiments. The plot of ratio versus nucleotide length from the *in vitro* RNA folding experiment resulted in a descending trend (Figure 5a), which was not observed for *in vivo* samples. The results suggest that RNA folding *in vivo* and *in vitro* are not always identical. Correctly folded *5′+12* or *5′+15* RNA were significantly recovered after denaturation and refolding (Figure 3b). However, the misfolded *in vivo 5′+12* and *5′+15* RNA constructs, if any, could not be recovered upon refolding (Figure 6c).

Comparison of the sequences with their complementary partners

The folding properties of discontinuous 3WJ-pRNA were further analyzed by a prediction algorithm using free energy minimization parameters and *mfold* (4). The goal was to investigate how different lengths at the 5′-end contributed to the disruption of the 3WJ-pRNA constructs, and whether there was a relationship between this influence and the predicted free energy of the added sequences on their partners. The following free energies for the duplexes of 5′- or 3′-end overhanging sequences and their complementary partners were calculated at 10^{-4} M RNA in the presence of 1 M NaCl:

$\Delta G = -6.1$ kcal/mole for the *5′+6* RNA
$\Delta G = -19.4$ kcal/mol for the *5′+12* RNA
$\Delta G = -25.6$ kcal/mol for the *5′+15* RNA
$\Delta G = -26.6$ kcal/mol for the *3′+15* RNA (control)

The longest construct with a 15-nt complementary sequence had the highest stability with a ΔG of −25.6 kcal/mol. This indicates that the folding of the 3WJ-pRNA complex *5′+15* during *in vitro* transcription was strongly interfered. This theoretical data was consistent with the correlation observed by fluorescence measurements of 'r' values. The 3′-end interfering sequences resulted in the lowest free energy value, ΔG = −26.6 kcal/mol. This sequence did not interfere with the MG fluorescence signal since the transcription reaction occurs from the 5′ to the 3′-end, and the 15-nt region was produced after the 3WJ complex had folded.

DISSCUSION

With the recent emergence of RNA nanotechnology (2), development of new systems to investigate the folding of RNA nanostructures has become very desirable. It has been reported that RNA junction motifs, such as 3WJs, 4WJs, and 5WJs can form rigid structures composed of discontinued RNA fragments (6, 8,10,11). The application of robust RNA motifs as vectors to carry exogenous functional moieties has been reported (23,6,8,12,48). The novelty here is not the application of the RNA motif as vector, but the use of the unique pRNA-3WJ with favorable thermodynamic attributes to drive the assembly of fusion RNA complexes (6,8). The energy landscape in RNA folding remains fundamentally important. When many motifs with similar levels of folding energies are fused into one large RNA molecule, new complementary sequences will appear and redistribution of energy landscape following the nearest neighboring principle will occur.

The pRNA-3WJ motif can be assembled from three pieces of RNA oligonucleotides with a T_M slope close to 90° (6,8). The resulting three-component complex was resistant to 8 M Urea denaturation and does not dissociate

at extremely low concentrations (6,8). The three components had a much higher affinity for favorable interactions compared to any of the two components, indicating cooperative simultaneous folding of the three helical stems. The incorporation of a pRNA-3WJ with distinct low folding energy will provide a leading motif to drive the folding of other functional motifs with weaker folding forces. Thus, functional modules with weaker folding forces will be able to fold independently into their original authentic structure when linked to the branches of the pRNA-3WJ.

CONCLUSIONS

The thermodynamically ultrastable pRNA-3WJ motif of phi29 motor pRNA can be used to drive the folding of fused RNA molecules with controllable and predictable consequences. When a large fusion RNA molecule is constructed containing three individual 18-nt fragments dispersed at any location within the sequence, the three fragments drive the correct folding of other RNA functionalities or motifs into their original 3D structures with authentic functions. This approach offers a new system for future investigations into the important topic of RNA folding *in vivo*.

ACKNOWLEDGEMENTS

We thank Dr. Farzin Haque for insightful comments and Jeannie Haak for assistance in preparing this article.

FUNDING

National Institutes of Health (NIH) grants [EB003730 and CA151648 to P.G.] and The Arnold and Mabel Beckman fund [1210 to D.S.]. Funding to Peixuan Guo's Endowed Chair in Nanobiotechnology position is by the William Fairish Endowment Fund. P.G. is a cofounder of Kylin Therapeutics, Inc., and Biomotor and Nucleic Acid Nanotechnology Development Corp. Ltd. Funding for open access charge: NIH [EB003730 and CA151648 to P.G.].

Conflict of interest statement. P.G. is a cofounder of Kylin Therapeutics, Inc. and Biomotor and Nucleic Acid Nanotechnology Development Corp. Ltd.

REFERENCES

1. Guo,P., Zhang,C., Chen,C., Trottier,M. and Garver,K. (1998) Inter-RNA interaction of phage phi29 pRNA to form a hexameric complex for viral DNA transportation. *Mol. Cell.*, **2**, 149–155.
2. Guo,P. (2010) The emerging field of RNA nanotechnology. *Nature Nanotechnology*, **5**, 833–842.
3. Markham,N.R. and Zuker,M. (2008) UNAFold: software for nucleic acid folding and hybridization. *Methods Mol. Biol.*, **453**, 3–31.
4. Zuker,M. (2003) Mfold web server for nucleic acid folding and hybridization prediction. *Nucleic Acids Res.*, **31**, 3406–3415.
5. Chan,L., Zuker,M. and Jacobson,A.B. (1990) A computer method for finding common base paired helices in aligned sequences: application to the analysis of random sequences. *Nucleic Acids Res.*, **19**, 353–358.
6. Shu,D., Shu,Y., Haque,F., Abdelmawla,S. and Guo,P. (2011) Thermodynamically stable RNA three-way junctions for constructing multifuntional nanoparticles for delivery of therapeutics. *Nature Nanotechnology*, **6**, 658–667.
7. Reif,R., Haque,F. and Guo,P. (2013) Fluorogenic RNA nanoparticles for monitoring RNA Folding and degradation in real time in living cells. *Nucleic Acid Ther.*, **22**, 428–437.
8. Haque,F., Shu,D., Shu,Y., Shlyakhtenko,L., Rychahou,P., Evers,M. and Guo,P. (2012) Ultrastable synergistic tetravalent RNA nanoparticles for targeting to cancers. *Nano Today*, **7**, 245–257.
9. Felden,B., Florentz,C., Giegé,R. and Westhof,E. (1996) A central pseudoknotted three-way junction imposes tRNA-like mimicry and the orientation of three 5′ upstream pseudoknots in the 3′ terminus of tobacco mosaic virus RNA. *RNA*, **2**, 201–212.
10. Nasalean,L., Baudrey,S., Leontis,N.B. and Jaeger,L. (2006) Controlling RNA self-assembly to form filaments. *Nucleic Acids Res.*, **34**, 1381–1392.
11. Severcan,I., Geary,C., Verzemnieks,E., Chworos,A. and Jaeger,L. (2009) Square-shaped RNA particles from different RNA folds. *Nano Lett.*, **9**, 1270–1277.
12. Shu,Y., Haque,F., Shu,D., Li,W., Zhu,Z., Kotb,M., Lyubchenko,Y. and Guo,P. (2013) Fabrication of 14 Different RNA nanoparticles for specific tumor targeting without accumulation in normal organs. *RNA*, **19**, 766–777.
13. Grabow,W.W., Zakrevsky,P., Afonin,K.A., Chworos,A., Shapiro,B.A. and Jaeger,L. (2011) Self-assembling RNA nanorings based on RNAI/II inverse kissing complexes. *Nano Lett.*, **11**, 878–887.
14. Ohno,H., Kobayashi,T., Kabata,R., Endo,K., Iwasa,T., Yoshimura,S.H., Takeyasu,K., Inoue,T. and Saito,H. (2011) Synthetic RNA-protein complex shaped like an equilateral triangle. *Nat. Nanotechnol.*, **6**, 116–120.
15. Schroeder,K.T., McPhee,S.A., Ouellet,J. and Lilley,D.M. (2010) A structural database for k-turn motifs in RNA. *RNA.*, **16**, 1463–1468.
16. Ishikawa,J., Fujita,Y., Maeda,Y., Furuta,H. and Ikawa,Y. (2010) GNRA/receptor interacting modules: Versatile modular units for natural and artificial RNA architectures. *Methods*, **54**, 226–238.
17. Novikova,I.V., Hassan,B.H., Mirzoyan,M.G. and Leontis,N.B. (2010) Engineering cooperative tecto-RNA complexes having programmable stoichiometries. *Nucleic Acids Res.*, **39**, 2903–2917.
18. Shu,D., Moll,W.D., Deng,Z., Mao,C. and Guo,P. (2004) Bottom-up assembly of RNA arrays and superstructures as potential parts in nanotechnology. *Nano Lett.*, **4**, 1717–1723.
19. Khaled,A., Guo,S., Li,F. and Guo,P. (2005) Controllable self-assembly of nanoparticles for specific delivery of multiple therapeutic molecules to cancer cells using RNA nanotechnology. *Nano Letters*, **5**, 1797–1808.
20. Guo,P. (2005) RNA nanotechnology: engineering, assembly and applications in detection, gene delivery and therapy. *J. Nanosci. Nanotechnol.*, **5**, 1964–1982.
21. Guo,S., Huang,F. and Guo,P. (2006) Construction of folate-conjugated pRNA of bacteriophage phi29 DNA packaging motor for delivery of chimeric siRNA to nasopharyngeal carcinoma cells. *Gene Ther.*, **13**, 814–820.
22. Abdelmawla,S., Guo,S., Zhang,L., Pulukuri,S., Patankar,P., Conley,P., Trebley,J., Guo,P. and Li,Q.X. (2011) Pharmacological characterization of chemically synthesized monomeric pRNA nanoparticles for systemic delivery. *Mol. Ther.*, **19**, 1312–1322.
23. Ponchon,L. and Dardel,F. (2011) Large scale expression and purification of recombinant RNA in Escherichia coli. *Methods*, **54**, 267–273.
24. Taft,R.J., Pang,K.C., Mercer,T.R., Dinger,M. and Mattick,J.S. (2010) Non-coding RNAs: regulators of disease. *J. Pathol.*, **220**, 126–139.
25. Duchaine,T.F. and Slack,F.J. (2009) RNA interference and micro-RNA-oriented therapy in cancer: rationales, promises, and challenges. *Curr. Oncol.*, **16**, 265–270.

26. Cayrol,B., Nogues,C., Dawid,A., Sagi,I., Silberzan,P. and Isambert,H. (2009) A nanostructure made of a bacterial noncoding RNA. *J. Am. Chem. Soc.*, **131**, 17270–17276.
27. Mattick,J.S. (2009) The genetic signatures of noncoding RNAs. *PLoS. Genet.*, **5**, e1000459.
28. Schroeder,R., Grossberger,R., Pichler,A. and Waldsich,C. (2002) RNA folding in vivo. *Curr. Opin. Struct. Biol.*, **12**, 296–300.
29. Donahue,C.P., Yadava,R.S., Nesbitt,S.M. and Fedoruk,M.N. (2000) The kinetic mechanism of the hairpin ribozyme in vivo: influence of RNA helix stability on intracellular cleavage kinetics. *J. Mol. Biol.*, **295**, 693–707.
30. Donahue,C.P. and Fedor,M.J. (1997) Kinetics of hairpin ribozyme cleavage in yeast. *RNA*, **3**, 961–973.
31. Babendure,J.R., Adams,S.R. and Tsien,R.Y. (2003) Aptamers switch on fluorescence of triphenylmethane dyes. *J. Am. Chem. Soc.*, **125**, 14716–14717.
32. Afonin,K.A., Danilov,E.O., Novikova,I.V. and Leontis,N.B. (2008) TokenRNA: A new type of sequence-specific, label-free fluorescent biosensor for folded RNA molecules. *Chembiochem*, **9**, 1902–1905.
33. Knapp,G. (1989) Enzymatic approaches to probing of RNA secondary and tertiary structure. *Methods Enzymol.*, **180**, 192–212.
34. Peattie,D.A. and Gilbert,W. (1980) Chemical probes for higher-order structure in RNA. *Proc. Natl Acad. Sci. USA*, **77**, 4679–4682.
35. Trottier,M., Mat-Arip,Y., Zhang,C., Chen,C., Sheng,S., Shao,Z. and Guo,P. (2000) Probing the structure of monomers and dimers of the bacterial virus phi29 hexamer RNA complex by chemical modification. *RNA*, **6**, 1257–1266.
36. Zhang,C., Trottier,M., Chen,C. and Guo,P. (2001) Chemical modification patterns of active and inactive as well as procapsid-bound and unbound DNA-packaging RNAof bacterial virus Phi29. *Virology*, **281**, 281–293.
37. Mat-Arip,Y., Garver,K., Chen,C., Sheng,S., Shao,Z. and Guo,P. (2001) Three-dimensional interaction of Phi29 pRNA dimer probed by chemical modification interference, cryo-AFM, and cross-linking. *J. Biol. Chem.*, **276**, 32575–32584.
38. Krol,A. and Carbon,P. (1989) A guide for probing native small nuclear RNA and ribonucleoprotein structures. *Meth. Enzymol.*, **180**, 213–227.
39. Ehresmann,C., Baudin,F., Mougel,M., Romby,P., Ebel,J.-P. and Ehresmann,B. (1987) Probing the structure of RNAs in solution. *Nucleic Acids Res.*, **15**, 9109–9128.
40. Moazed,U., Stern,S. and Noller,H.F. (1986) Rapid chemical probing of conformation in 16S ribosomal RNA and 30S ribosomal subunits using primer extension. *J. Mol. Biol.*, **187**, 399–416.
41. Lindell,M., Romby,P. and Wagner,E.G. (2002) Lead(II) as a probe for investigating RNA structure in vivo. *RNA*, **8**, 534–541.
42. Wang,X.D. and Padgett,R.A. (1989) Hydroxyl radical "footprinting" of RNA: application to pre-mRNA splicing complexes. *Proc. Natl Acad. Sci.*, **86**, 7795–7799.
43. Zhang,H., Endrizzi,J.A., Shu,Y., Haque,F., Sauter,C., Shlyakhtenko,L.S., Lyubchenko,Y., Guo,P. and Chi,Y.I. (2013) Crystal structure of 3WJ core revealing divalent ion-promoted thermostability and assembly of the Phi29 hexameric motor pRNA. *RNA*, **19**, 1226–1237.
44. Shu,D., Huang,L., Hoeprich,S. and Guo,P. (2003) Construction of phi29 DNA-packaging RNA (pRNA) monomers, dimers and trimers with variable sizes and shapes as potential parts for nano-devices. *J. Nanosci. Nanotechnol.*, **3**, 295–302.
45. Hoeprich,S., ZHou,Q., Guo,S., Qi,G., Wang,Y. and Guo,P. (2003) Bacterial virus phi29 pRNA as a hammerhead ribozyme escort to destroy hepatitis B virus. *Gene Ther.*, **10**, 1258–1267.
46. Feng,Y., Kong,Y.Y., Wang,Y. and Qi,G.R. (2001) Inhibition of hepatitis B virus by hammerhead ribozyme targeted to the poly(A) signal sequence in cultured cells. *Biol Chem*, **382**, 655–660.
47. Ponchon,L. and Dardel,F. (2007) Recombinant RNA technology: the tRNA scaffold. *Nat Methods*, **4**, 571–576.
48. Shu,Y., Shu,D., Haque,F. and Guo,P. (2013) Fabrication of pRNA nanoparticles to deliver therapeutic RNAs and bioactive compounds into tumor cells. *Nat Protoc.*, **8**, 1635–1659.
49. Ambrosini,G., Adida,C., Sirugo,G. and Altieri,D.C. (1998) Induction of apoptosis and inhibition of cell proliferation by survivin gene targeting. *J. Biol. Chem.*, **273**, 11177–11182.
50. Ambrosini,G., Adida,C. and Altieri,D.C. (1997) A novel anti-apoptosis gene, survivin, expressed in cancer and lymphoma. *Nat. Med.*, **3**, 917–921.
51. Baugh,C., Grate,D. and Wilson,C. (2000) 2.8 A crystal structure of the malachite green aptamer. *J. Mol. Biol.*, **301**, 117–128.
52. Paige,J.S., Wu,K.Y. and Jaffrey,S.R. (2011) RNA mimics of green fluorescent protein. *Science*, **333**, 642–646.
53. Srisawat,C. and Engelke,D.R. (2001) Streptavidin aptamers: affinity tags for the study of RNAs and ribonucleoproteins. *RNA*, **7**, 632–641.
54. Lu,Y. and Low,P.S. (2002) Folate-mediated delivery of macromolecular anticancer therapeutic agents. *Adv. Drug Deliv. Rev.*, **54**, 675–693.
55. Puglisi,J.D., Wyatt,J.R. and Tinoco,I. Jr (1988) A pseudoknotted RNA oligonucleotide. *Nature*, **331**, 283–286.
56. Isambert,H. (2009) The jerky and knotty dynamics of RNA. *Methods*, **49**, 189–196.
57. Mathews,D.H. and Turner,D.H. (2006) Prediction of RNA secondary structure by free energy minimization. *Curr. Opin. Struct. Biol.*, **16**, 270–278.
58. Bindewald,E., Afonin,K., Jaeger,L. and Shapiro,B.A. (2011) Multistrand RNA secondary structure prediction and nanostructure design including pseudoknots. *ACS Nano.*, **5**, 9542–9551.
59. Pleij,C.W.A., Rietveld,K. and Bosch,L. (1985) A new principle of RNA folding based on pseudonotting. *Nucleic Acids Res.*, **13**, 1717–1731.
60. Milligan,J.F., Groebe,D.R., Witherell,G.W. and Uhlenbeck,O.C. (1987) Oligoribonucleotide synthesis using T7 RNA polymerase and synthetic DNA templates. *Nucleic Acid Res.*, **15**, 8783–8798.
61. He,Y.K., Lu,C.D. and Qi,G.R. (1993) In vitro cleavage of HPV16 E6 and E7 RNA fragments by synthetic ribozymes and transcribed ribozymes from RNA-trimming plasmids. *FEBS Lett.*, **322**, 21–24.